ACCESS CellPress
Cell Reports
Article

RNA Helicases DDX5 and DDX17 Dynamically Orchestrate Transcription, miRNA, and Splicing Programs in Cell Differentiation

Etienne Dardenne,[1,2,3,4,5] Micaela Polay Espinoza,[1,2,3,4,5] Laurent Fattet,[1,2,3,4] Sophie Germann,[1,2,3,4] Marie-Pierre Lambert,[1,2,3,4] Helen Neil,[1,2,3,4] Eleonora Zonta,[1,2,3,4] Hussein Mortada,[1,2,3,4] Lise Gratadou,[1,2,3,4] Mathieu Deygas,[1,2,3,4] Fatima Zahra Chakrama,[1,2,3,4] Samaan Samaan,[1,2,3,4] François-Olivier Desmet,[1,2,3,4] Léon-Charles Tranchevent,[1,2,3,4] Martin Dutertre,[1,2,3,4] Ruth Rimokh,[1,2,3,4] Cyril F. Bourgeois,[1,2,3,4,*] and Didier Auboeuf[1,2,3,4,*]
[1]INSERM U1052, Centre de Recherche en Cancérologie de Lyon, 69008 Lyon, France
[2]CNRS UMR5286, Centre de Recherche en Cancérologie de Lyon, 69008 Lyon, France
[3]Université Claude Bernard Lyon 1, 69008 Lyon, France
[4]Centre Léon Bérard, 69008 Lyon, France
[5]Co-first author
*Correspondence: cyril.bourgeois@inserm.fr (C.F.B.), didier.auboeuf@inserm.fr (D.A.)
http://dx.doi.org/10.1016/j.celrep.2014.05.010

SUMMARY

The RNA helicases DDX5 and DDX17 are members of a large family of highly conserved proteins that are involved in gene-expression regulation; however, their in vivo targets and activities in biological processes such as cell differentiation, which requires reprogramming of gene-expression programs at multiple levels, are not well characterized. Here, we uncovered a mechanism by which DDX5 and DDX17 cooperate with heterogeneous nuclear ribonucleoprotein (hnRNP) H/F splicing factors to define epithelial- and myoblast-specific splicing subprograms. We then observed that downregulation of DDX5 and DDX17 protein expression during myogenesis and epithelial-to-mesenchymal transdifferentiation contributes to the switching of splicing programs during these processes. Remarkably, this downregulation is mediated by the production of miRNAs induced upon differentiation in a DDX5/DDX17-dependent manner. Since DDX5 and DDX17 also function as coregulators of master transcriptional regulators of differentiation, we propose to name these proteins "master orchestrators" of differentiation that dynamically orchestrate several layers of gene expression.

INTRODUCTION

Transcriptome reprogramming during cell differentiation involves multiple layers of regulation of the gene-expression process, including transcription, alternative splicing that expands the gene message, and miRNAs that control mRNA stability and translation (Ebert and Sharp, 2012; Kalsotra and Cooper, 2011). These different gene-expression layers are usually analyzed independently, even though many factors that participate in several of these layers have been identified. Yet, evidence that a single factor orchestrates several gene-expression layers during cell differentiation is still lacking.

The DEAD box RNA helicase DDX5 and its paralog, DDX17, are highly conserved proteins that function in most steps of the gene-expression process, although their in vivo targets and activities are not fully characterized (Fuller-Pace and Moore, 2011; Janknecht, 2010; Linder and Jankowsky, 2011). They are coregulators of several transcription factors, including MYOD, a master regulator of muscle differentiation (Caretti et al., 2006), and SMAD proteins (Warner et al., 2004; Davis et al., 2008), which mediate transforming growth factor β (TGF-β)-induced epithelial-to-mesenchymal transition (EMT), i.e., the transdifferentiation of epithelial cells to fibroblasts (Thiery et al., 2009). In addition, DDX5 and DDX17 control the biogenesis of miRNAs via their interaction with the Drosha/DGCR8 complex (Fukuda et al., 2007, Suzuki et al., 2009). Finally, DDX5 and DDX17 are also components of the spliceosome and regulate alternative splicing (Dardenne et al., 2012; Germann et al., 2012; Lin et al., 2005; Samaan et al., 2014).

Two mutually nonexclusive models have been proposed to explain the role of DDX5 and DDX17 in alternative splicing. First, DDX5 and DDX17 may modulate splicing decisions owing to their ability to actively unwind the duplex between the U1 small nuclear RNA (snRNA) and the 5′ splice site (5′ss), favoring the transition from the pre- to active spliceosome (Lin et al., 2005). Second, DDX5 and DDX17 have been shown in two gene models (H-*ras* and *Tau*) to impact RNA secondary structures that modulate access of the U1 snRNA to the 5′ss or access of the RBM4 splicing regulator to its binding site downstream of a weak 5′ss (Camats et al., 2008; Kar et al., 2011). Whether DDX5 and DDX17 influence a specific class of secondary structure is not known. However, in both models the RNA helicase activity of DDX5 and DDX17 is required and the 5′ss seems to be the preferential target of these factors. In addition, these models point to

a role of DDX5/DDX17 in controlling the kinetics of splicing by favoring either the transition between different states of the spliceosome or the recruitment of splicing factors downstream of the 5′ss.

In this report, we demonstrate that DDX5 and DDX17 cooperate with heterogeneous nuclear ribonucleoprotein (hnRNP) H/F splicing regulators at the level of 5′ss located in regions that are prone to form G-quadruplex structures. This cooperation helps to establish specific splicing subprograms in epithelial cells and myoblasts. We next show that the downregulation of DDX5/DDX17 expression observed during EMT and myogenesis contributes to the reprogramming of splicing during these processes. Importantly, this downregulation is mediated by specific miRNAs whose biogenesis requires both DDX5 and DDX17. Finally, we show that DDX5 and DDX17 are required to initiate EMT and myogenesis as transcriptional coregulators of SMADs and MyoD, respectively, driving the production of key secondary differentiation regulators. We propose a model in which DDX5 and DDX17 directly and dynamically orchestrate transcription, miRNA, and splicing programs in cell differentiation.

RESULTS

DDX5 and DDX17 Regulate Alternative Splicing of Exons Exhibiting Specific Features

In order to assess the role of DDX5 and DDX17 in splicing, we performed a genome-wide study using Affymetrix Human Exon Arrays on epithelial MCF7 breast cancer cells transfected with small interfering RNAs (siRNAs) targeting both *DDX5* and *DDX17* (si*DDX5/17*) or a control siRNA (Figure 1A). Among the regulated single cassette exons, 63% (233) were more skipped and 37% (139) were more included following DDX5/DDX17 depletion (Figure 1B; Table S1). Hereafter, "class S" and "class I" exons will respectively refer to skipped and included exons upon DDX5/DDX17 depletion. As shown in Figures 1C and S1A, there was a good correlation between Exon Array prediction and extensive RT-PCR validation (n = 121).

While analyzing DDX5/DDX17-regulated exons by RT-PCR, we observed that class I exons had a low basal inclusion rate in control cells (Figures 1C and 1D). We confirmed this observation by examining the computed inclusion rate of DDX5/DDX17-regulated exons using gene-normalized exon intensities from our microarray data sets (Figure S1B) or by computing their inclusion rate from the corresponding mRNAs annotated in public libraries (Figure S1C). The poor inclusion of class I exons is explained by the fact that they have weak 5′ss and 3′ss compared with both constitutive (CONS) and alternative (ALT) exons (Figures 1E and S1D). These exons are also flanked by large introns (Figure 1F).

Class S exons have very different features (Figure 1H). First, they are highly included in control cells (Figures 1C and 1D, S1B, and S1C). They are flanked by short introns and have strong 3′ss (Figures 1F and S1D). In addition, the 5′ss of class S exons is embedded in GC-rich sequences, in contrast to the 5′ss of class I exons (Figure 1G). However, similarly to class I exons, class S exons harbor weak 5′ss (Figure 1E).

DDX5/DDX17 and hnRNP H/F Regulate the Same Subset of Exons

Because class S exons are highly included in control cells despite their weak 5′ss, we hypothesized that 5′ss activators may enhance their inclusion in a DDX5/DDX17-dependent manner. To test this hypothesis, we computed the density of previously reported intronic splicing enhancers (ISE) downstream of the 5′ss regulated by DDX5 and DDX17 (Lim and Burge, 2001; Zhang et al., 2005). As shown in Figure S1E, there is an enrichment of ISE downstream of class S exons compared with control sets of alternative and constitutive exons. We then used the SFmap software (Paz et al., 2010) to search for specific ISE motifs. Because class S 5′ss were embedded in GC-rich sequences (Figure 1G), we focused our attention on splicing factors with a known affinity for GC-rich motifs, such as hnRNP H/F (Huelga et al., 2012; Katz et al., 2010; Xiao et al., 2009). Clearly, there is an enrichment in hnRNP H/F binding motifs downstream of class S exons (Figure S1E).

Supporting an important functional connection between DDX5/DDX17 and hnRNP H/F, an analysis of a previously published RNA sequencing (RNA-seq) data set (Xiao et al., 2009) showed that at least 60 of the 233 class S exons (i.e., skipped upon DDX5/DDX17 depletion) were also skipped following hnRNP H1 depletion (Table S2). In addition, analysis of existing crosslinking immunoprecipitation sequencing (CLIP-seq) data sets (Huelga et al., 2012; Katz et al., 2010) revealed that those 60 exons, as well as the complete set of 233 class S exons, are flanked by a larger number of hnRNP H/F CLIP-seq reads than a control set of randomly selected alternative exons (Figure 2A; Table S2). Remarkably, joint hnRNP H/F and DDX5/DDX17 depletion (Figure S1F) cooperatively enhanced the skipping of exons containing hnRNP H/F binding sites, but not of control exons without hnRNP H/F binding sites (Figures 2B and 2C).

Intriguingly, while analyzing the environment of class I exons, we observed that the 5′ss of exons (n − 1), i.e., located just upstream of class I exons (n), present features similar to the 5′ss of class S exons (n): they are embedded in GC-rich sequences (Figure 2D) and they are enriched in intronic hnRNP H/F binding sites (Figure 2E). Based on the similar 5′ss configuration of class I exons (n − 1) and class S exons (n), and on recent kinetic models of splicing regulation (Schor et al., 2013), we hypothesized that in the case of class I exons, the depletion of DDX5/DDX17 and/or hnRNP H/F could slow down splicing of exon (n − 1) to exon (n + 1), and consequently increase the time window for recognition and inclusion of the weak exon (n). To test this model, we selected a set of class I exons with or without hnRNP H/F binding sites downstream of exon (n − 1). Remarkably, hnRNP H/F depletion, by itself or together with DDX5/DDX17 depletion, enhanced exon (n) inclusion only when hnRNP H/F binding sites were present downstream of exon (n − 1) (Figure 2E).

We next reasoned that if DDX5/DDX17 depletion would slow down exon (n − 1) to exon (n + 1) splicing, this would give enough time for splicing activators to enhance weak exon (n) inclusion. As the 5′ss of class I exons are followed by GC-poor sequences, we looked for TIA1 and TIAL1 binding sites because these factors bind to AT-rich motifs (Wang et al., 2010b; Figure 1F). Analysis

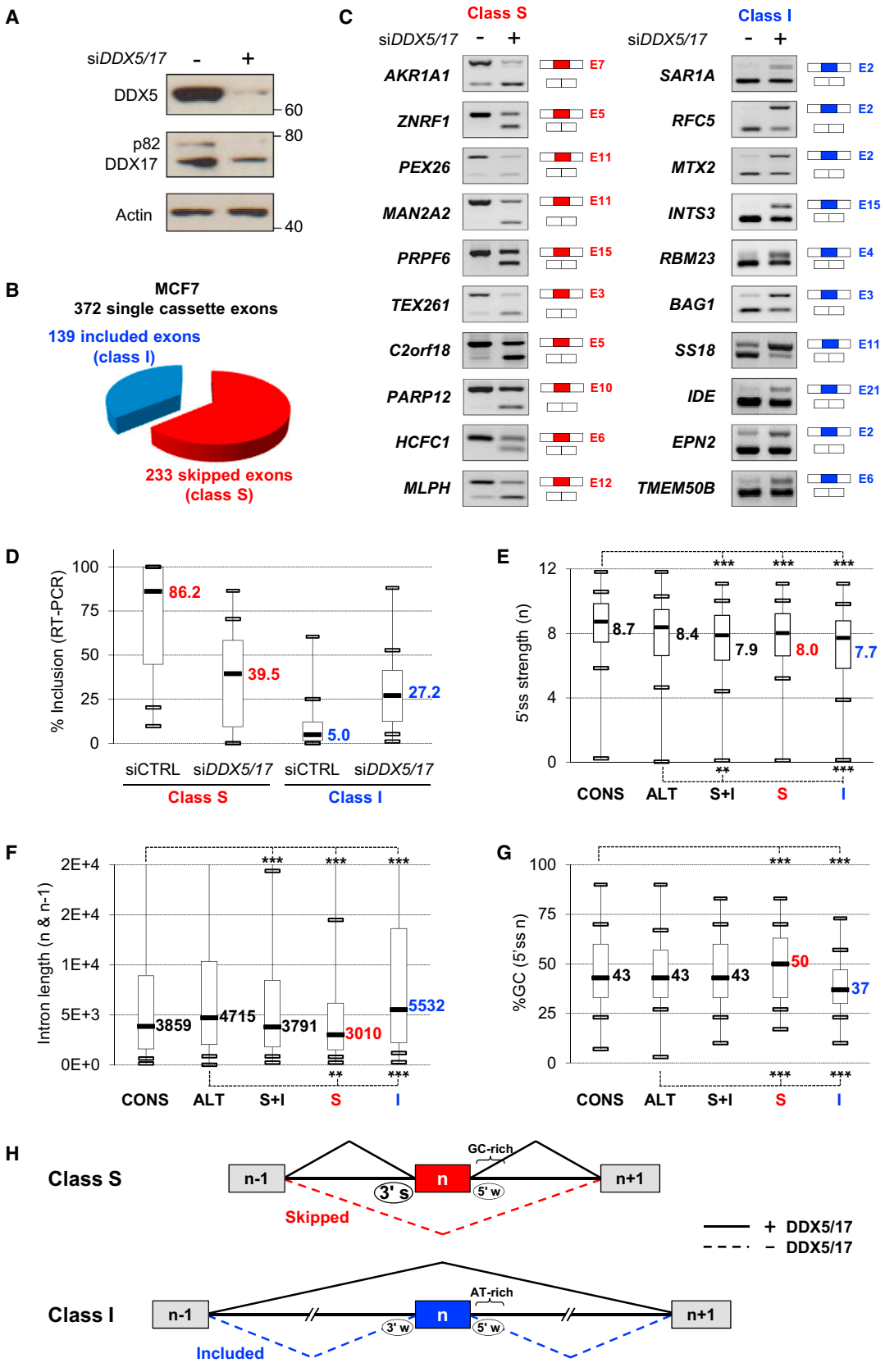

(legend on next page)

of available CLIP-seq data sets revealed an enrichment of TIA1 binding sites downstream of class I exons (Figure 2F; Table S2). Furthermore, TIA1/TIAL1 depletion (Figure S1G) reduced DDX5/DDX17-mediated exon inclusion only when TIA1/TIAL1 binding sites were found downstream of the regulated exons, but not in a control exon (Figure 2G). It must be underlined that DDX5/DDX17 depletion slightly decreased TIA1 and TIAL1 protein expression levels (Figure S1G). However, the effect of DDX5/DDX17 depletion on splicing could not be a consequence of TIA1/TIAL1 downregulation, because in that case the co-depletion of TIA1/TIAL1 and DDX5/DDX17 would have had similar effects and not antagonistic effects as shown in Figure 2G.

Cooperation between DDX5/DDX17 and hnRNP H/F on G-Quadruplex Structures

It was previously shown that hnRNP H/F binds to G-tracts that can form G-quadruplexes (Decorsière et al., 2011). Interestingly, the high kinetic stability of a G-quadruplex limits hnRNP H/F binding to G-rich sequences (Samatanga et al., 2013). Computational analysis revealed an enrichment in predicted G-quadruplexes downstream of class S exons (n) when compared with class I exons (n) or a set of control exons (Figure 3A, right panel). Remarkably, an enrichment in G-quadruplexes was also predicted downstream of exons (n − 1) of class I exons compared with class S exons (n − 1) or a set of control exons (Figure 3A, left panel). Therefore, we hypothesized that the RNA helicase activity of DDX5 and DDX17 may favor the binding of hnRNP H/F to G-tracts embedded in G-quadruplex RNA structures.

Several lines of evidence support this hypothesis. First, in cellulo stabilization of G-quadruplex structures using the TMPyP4 reagent had the same effect on splicing as the silencing of *DDX5/DDX17* or *HNRNPH/F* genes (Figure 3B). Second, hnRNP H1 coimmunoprecipitated with both DDX5 and DDX17 (Figure 3C), in agreement with previous reports that suggested an interaction between these factors (Camats et al., 2008; Laurent et al., 2012). Such an interaction was further supported by an in situ proximity-ligation assay (PLA), a sensitive approach that uses rolling-circle amplification of fluorescent oligonucleotide probes linked to primary antibodies to reveal complexes between single molecules in close proximity (<40 nm) in cells. PLA using DDX5 and hnRNP H1 antibodies detected multiple spots in the nuclei of MCF7 cells (Figure 3D), which could reflect either a direct interaction or the close proximity of the two proteins bridged by RNA molecules. Third, an antibody against hnRNP H1 (but not a control antibody) immunoprecipitated their target RNAs, and DDX5/DDX17 depletion reduced this interaction (Figure 3E).

Finally, the helicase activity of DDX5 and DDX17 was required for the regulation of both exon inclusion and skipping. Stable inducible MCF7 cells were transfected with siRNAs targeting the UTR (5′ or 3′) of endogenous *DDX5* and *DDX17* mRNAs (si*DDX5/17*-UTR), which had the same effect as si*DDX5/17* (compare, for example, Figures 1C and 3F). Reexpression of wild-type DDX5 (Samaan et al., 2014) rescued the splicing pattern of the tested exons to a level close or identical to the control level (Figure 3F, lanes 1–3). In contrast, expression of a DDX5 mutant (DDX5-KA) lacking the helicase activity could not restore, or only partially restored, the splicing of the tested exons (Figure 3F, lanes 4–6). Similar results were obtained with DDX17 (Figure S1H), underlining the functional redundancy between the two proteins in splicing regulation.

Cooperation between DDX5/DDX17 and hnRNP H/F Contributes to Establish Epithelial- and Myoblast-Specific Splicing Programs

To confirm the cooperation between DDX5/DDX17 and hnRNP H/F in a different context, we performed a genome-wide analysis using Affymetrix Exon Arrays after DDX5/DDX17 depletion in MCF10A cells, another epithelial breast cell line (Figures 4A and S2A; Table S3). Remarkably, the DDX5/DDX17-regulated exons in MCF10A cells presented similar characteristics compared with DDX5/DDX17-regulated exons in MCF7 cells (Figures S2B–S2D). In addition, a subset of DDX5/DDX17-controlled exons were regulated by a cooperation between these RNA helicases and hnRNP H/F in MCF10A cells, as observed in MCF7 cells (Figure 4B). Finally, the in situ PLA confirmed the interaction between DDX5 and hnRNP H1 in MCF10A cells (Figure S2E).

MCF10A epithelial cells are particularly interesting because they can undergo EMT upon TGF-β treatment, a process that may involve DDX5, which has been shown to interact with SMAD proteins (Figure S3A) (Warner et al., 2004), the mediators of the cell response to TGF-β. Interestingly, we noticed that TGF-β treatment of MCF10A cells induced a decrease of DDX5

Figure 1. Genome-Wide Impact of DDX5/DDX17 on Splicing Defines Two Classes of Regulated Exons

(A) Western blot showing the expression of DDX5 and DDX17 in MCF7 cells 48 hr after transfection with a control siRNA (−) or with an siRNA targeting both *DDX5* and *DDX17* (si*DDX5/17*).

(B) Pie chart showing the number of skipped and included exons following DDX5/DDX17 depletion.

(C) RT-PCR validation of splicing events. Class S (skipped in the absence of DDX5/DDX17) and class I (included in the absence of DDX5/DDX17) exons are in red and blue, respectively. The exon number is indicated.

(D) Boxplot representing the percentage of exon inclusion obtained by RT-PCR in control (siCTRL) and si*DDX5/17* conditions.

(E) Boxplot representing the 5′ss strength of class S (S) and class I (I) exons or the total of both classes (S+I), as well as control sets of constitutive (CONS) or alternative (ALT) exons.

(F) Boxplot representing the average length of introns upstream and downstream of the indicated exons (defined as in E).

(G) Boxplot representing the percentage of G/C nucleotides within the 30-nt-long region downstream of the 5′ss of the indicated exons (as in E).

(H) Schematic representation of DDX5/DDX17-regulated exon features. The skipped exons (n in red) have a weak 5′ss (5′w), a strong 3′ss (3′s), and a downstream GC-rich region. The included exons (n in blue) have a weak 5′ss (5′w), a weak 3′ss (3′w), and a downstream AT-rich region. The introns surrounding skipped exons are smaller than the introns surrounding included exons. $^{**}p < 0.01$, $^{***}p < 0.001$; Wilcoxon rank sum test.

See also Figure S1 and Table S1.

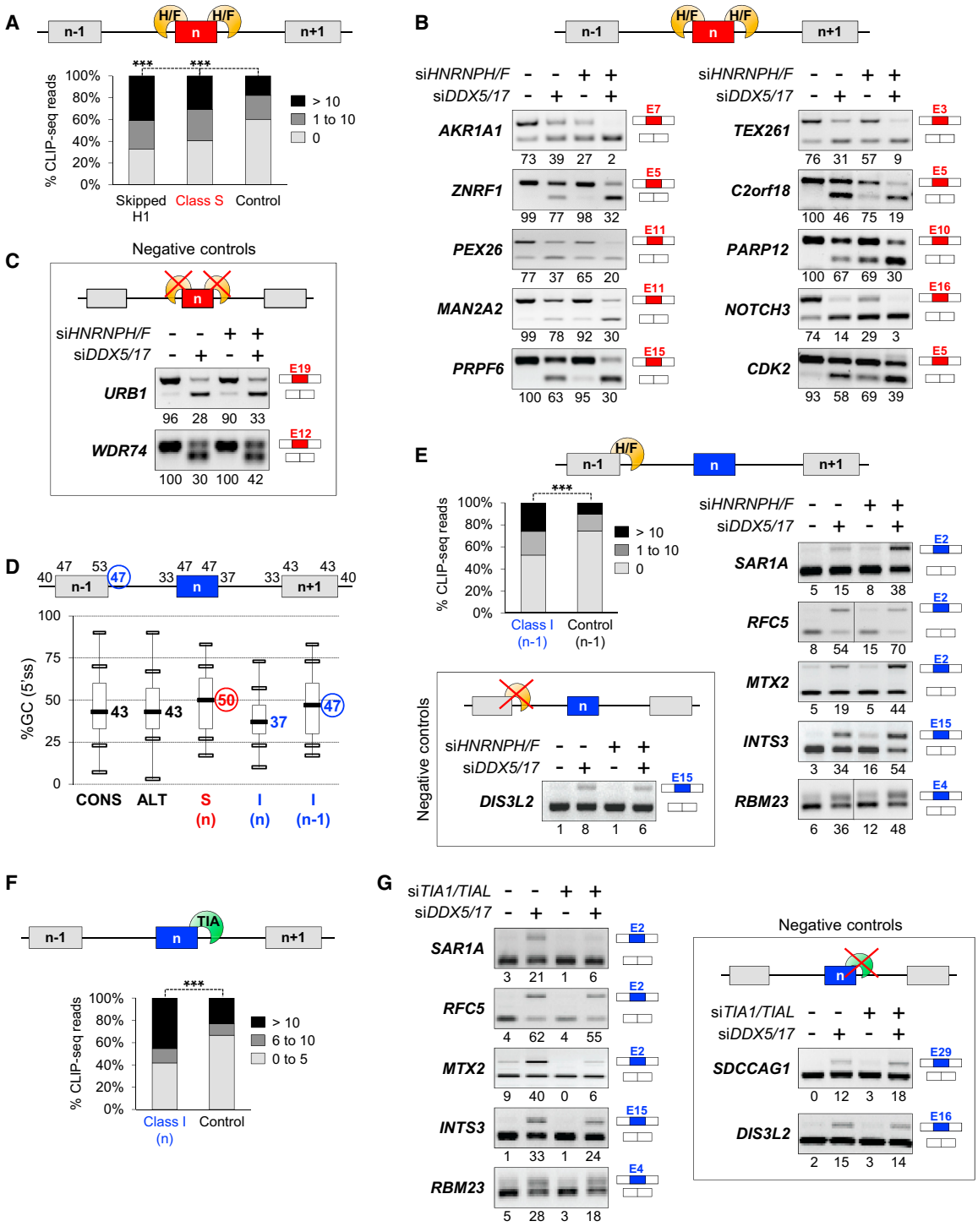

Figure 2. The Localization of GC-Rich hnRNP H/F Binding Sites Defines the Splicing Outcome of the Two Classes of DDX5/DDX17-Regulated Exons

(A) A 100% stacked bar chart representing the percentage of exons with hnRNP H1/F CLIP-seq reads. Three classes of exons were defined: a subset of experimentally validated 60 hnRNP H1-dependent class S exons (skipped H1), the total pool of class S exons (class S), and a panel of 985 alternative exons (Control). The distribution of the number of reads within regions of 500 nt upstream and/or downstream of tested exons was classified into three groups: no read (0), one to 10 reads, and more than 10 reads localized (***$p < 0.001$, χ^2 test).

(B) RT-PCR analysis of the effect of DDX5/DDX17 and/or hnRNP H/F depletion on class S exons enriched in hnRNP H1/F binding sites. PCR gels are representative of three independent experiments. Quantification is shown as the percentage of alternative sequence inclusion (psi).

(legend continued on next page)

and DDX17 protein expression levels (Figure 4C). This prompted us to investigate the function of DDX5 and DDX17 during this process.

The decreased expression of DDX5/DDX17 led us to hypothesize that some alternative exons might be similarly affected by TGF-β treatment and siRNA-mediated *DDX5/DDX17* silencing. To test this hypothesis, we analyzed the effect of si*DDX5/DDX17*, in the absence of TGF-β treatment, on the inclusion of a set of exons previously reported to be regulated during EMT (Shapiro et al., 2011; Warzecha et al., 2010). Remarkably, a number of TGF-β-regulated exons were regulated similarly by DDX5/DDX17 depletion in untreated MCF10A cells (Figure 4D). Because some of these exons were also regulated in the same manner by hnRNP H/F depletion in the absence of TGF-β (Figure 4E), we concluded that the cooperation between DDX5/DDX17 and hnRNP H/F contributes to maintain an epithelial-specific splicing pattern and that DDX5/DDX17 downregulation during EMT contributes to switch splicing toward a fibroblast-like splicing program.

Based on a previous report (Caretti et al., 2006), we also investigated the role of Ddx5/Ddx17 in myogenesis using the well-studied mouse C2C12 myoblast cells. Strikingly, just as we found during TGF-β-mediated EMT, we observed a decreased expression of both Ddx5 and Ddx17 proteins upon induction of myoblast differentiation (Figure 4F). In a remarkable parallel to what we observed in MCF10A cells, a subset of exons that are regulated during differentiation of C2C12 cells (Bland et al., 2010) were regulated in the same manner upon *Ddx5/Ddx17* silencing in undifferentiated myoblasts (Figures 4G and S3B). Interestingly, more than half of these exons were also coregulated by hnRNP H/F (Figure 4G, right panel). Importantly, and as observed in MCF7 and MCF10A cells, Ddx5 and hnRNP H1 interacted directly in C2C12 cells (Figures S3C and S3D).

Altogether, these results support a model in which the cooperation between DDX5/DDX17 and hnRNP H/F helps to define epithelial- and myoblast-specific splicing subprograms. DDX5 and DDX17 downregulation may therefore contribute to the splicing changes that occur during EMT and myogenesis.

The Downregulation of DDX5 and DDX17 Is Part of a Feedback Regulatory Loop Involving miRNAs

Because the downregulation of DDX5 and DDX17 during EMT and myogenesis may appear contradictory to their previously reported function in these processes (Caretti et al., 2006; Yang et al., 2006), we sought to investigate the molecular mechanism that causes this downregulation. Interestingly, phylogenetically conserved binding sites for two miRNAs known to be upregulated during myogenesis, miR-1 and miR-206 (Rao et al., 2006), were predicted within the 3′ UTR of both *DDX5* and *DDX17* mRNAs (Figures S4A and S4B). Strikingly, overexpression of pre-miR-1 or pre-miR-206 in C2C12 cells reduced Ddx5 and Ddx17 protein levels (Figure 5A). Luciferase assays confirmed that this effect was mediated by a direct binding of miR-1/206 onto the predicted sites in mouse *Ddx5* and *Ddx17* 3′ UTRs (Figure 5B).

Induction of miR-1 and miR-206 expression during myogenesis is mediated at least in part by MyoD (Rao et al., 2006), which is coregulated by Ddx5 and Ddx17 (Caretti et al., 2006; Figure S5A). Remarkably, the induction of mature miR-1 and miR-206 during differentiation of C2C12 cells was prevented by Ddx5/Ddx17 depletion (Figure 5C, yellow). We observed a similar inhibition when we looked at the miRNA precursors pri-miR-1a1 and pri-miR-206 (Figure 5C, orange), indicating that the primary effect was a transcriptional inhibition of these miRNA genes. However, the partial repression of pri-miR-206 induction upon *Ddx5/Ddx17* silencing could also reflect an effect on the processing of miR-206 precursors, in agreement with previous reports (Fukuda et al., 2007; Suzuki et al., 2009; Hong et al., 2013). Yet, a direct transcriptional effect was strongly supported by the recruitment of Ddx5 to the promoters of both miR-1 and miR-206 coding genes (Figure 5D).

Several lines of evidence supported a similar feedback loop in MCF10A cells. First, the *DDX5* 3′ UTR contains two predicted binding sites for miR-181b (Figure S4A), which is known to be induced by TGF-β treatment (Wang et al., 2010a). Overexpression of pre-miR-181b in MCF10A cells reduced the DDX5 protein level (Figure 5E), and luciferase assays confirmed that this effect was mediated by a direct binding of miR-181b to the *DDX5* 3′ UTR, at least on the most conserved of the predicted sites (Figures 5F and S4A). Intriguingly, miR-181b also repressed endogenous DDX17 expression (Figure 5E), even though no miR-181b binding site was predicted within *DDX17* 3′ UTR (Figure S4B). This suggested either the existence of a noncanonical and/or nonpredicted binding site or an indirect regulation of DDX17 expression by miR-181b. Second, the TGF-β-induced expression of miR-181b in MCF10A cells was dependent on SMAD transcription factors (Figures S5B and S5C), which interact with DDX5 as described above (Figure S3A). As expected, TGF-β-induced miR-181b and pri-miR-181b expression was prevented by DDX5/DDX17 depletion (Figure 5G) and DDX5 was recruited on the promoter of the miR-181b-1 gene promoter

(C) Effect of hnRNP H/F on control class S exons without any CLIP-seq read.
(D) Upper panel: schematic representation of class I exons (n) with their upstream (n − 1) and downstream (n + 1) exons. The numbers correspond to the median %GC within 30 nt upstream or downstream of splice sites. Lower panel: boxplot as in Figure 1G, except that it also includes class I exons (n − 1). The median values for class S exon (n) and class I exons (n − 1) are circled in red and blue, respectively.
(E) Top-left panel: percentage of hnRNP H1/F CLIP-seq reads downstream of class I or control exons (n − 1). Details as described in (A). Right panel: effect of hnRNP H/F depletion on class I exons harboring hnRNP H1/F CLIP-seq reads downstream of their exon (n − 1). Bottom-left panel (framed): negative control (no CLIP-seq read).
(F) A 100% stacked bar chart representing the percentage of TIA1/TIAL1 CLIP-seq reads in a region of 700 nt downstream of class I exons (n) or control exons (n). Details as in (A).
(G) Left panel: RT-PCR analysis of the effect of TIA1/TIAL depletion on class I exons (n) containing TIA1/TIAL binding sites. Right panel (framed): negative controls (no CLIP-seq read).
See also Figures S1F and S1G, and Table S2.

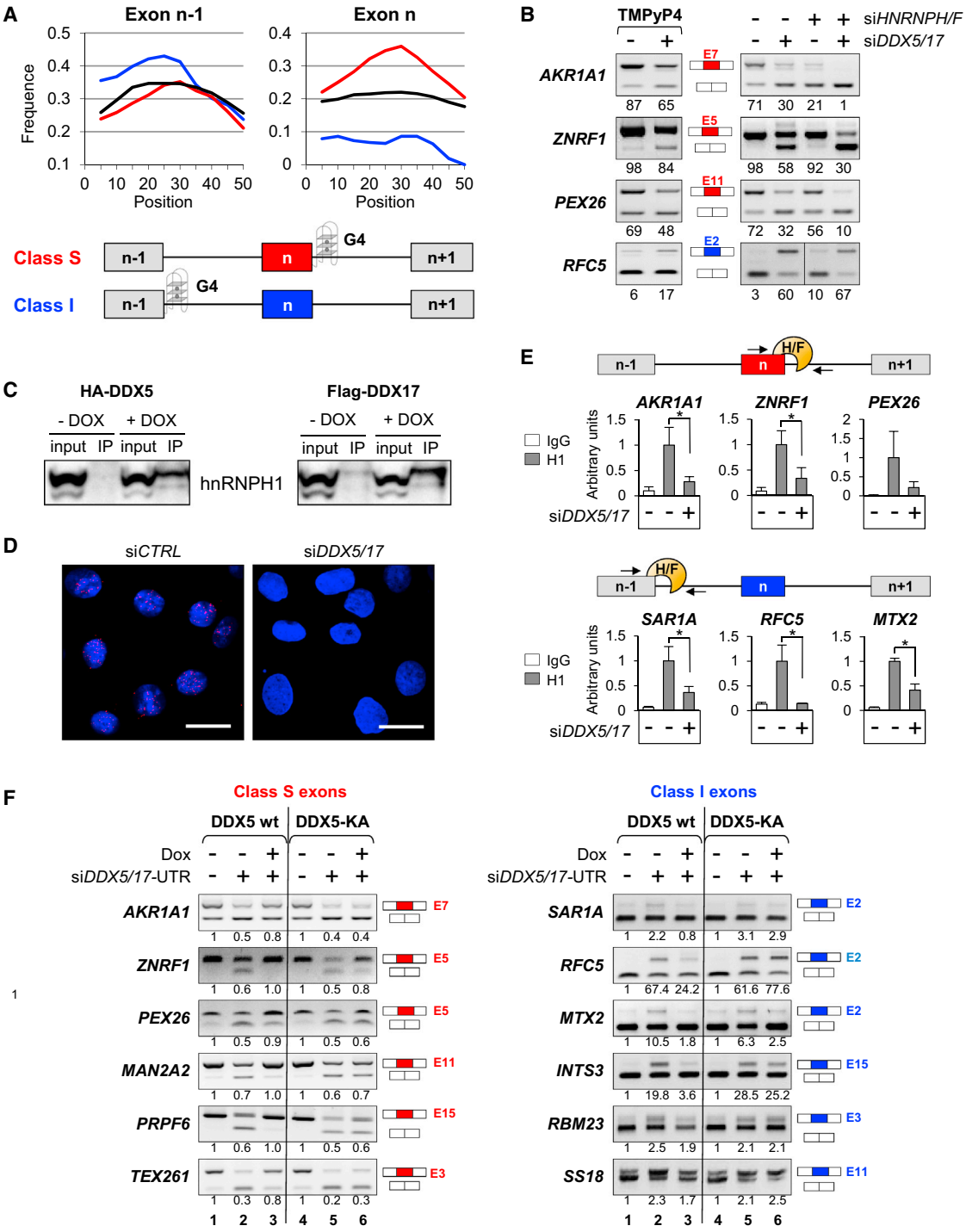

Figure 3. DDX5, DDX17, and hnRNP H/F Cooperate on G-Quadruplex Structures

(A) Prediction of G-quadruplex structures downstream of 5′ss of exons (n − 1) and (n) of class S (red line), class I (blue line), or control (black line) exons. Results of the predictions are schematized under the graphs.

(B) Splicing of alternative exons in MCF7 cells treated or not with TMPyP4 (left panel), or treated with si*DDX5/17* and/or si*HNRNPH/F* (as in Figure 2).

(C) Western blot analysis of hnRNP H1 after IP of cell lysates from stably induced (+ Dox) HA-DDX5 or FLAG-DDX17 MCF7 cell lines with HA (left) or FLAG (right) antibodies. Inputs (IN) correspond to 10% of total extract.

(D) In situ PLA showing the interaction between hnRNP H1 and DDX5 in the nuclei (stained with Hoechst) of MCF7 cells treated with control siRNA or si*DDX5/17*.

(E) qRT-PCR analysis after transfection with control siRNA (siCTRL) or si*DDX5/17*, and RNA-IP using control IgG antibody or hnRNP H1 antibodies. Amplification was performed with primers (arrows) encompassing the 5′ss of class S exon (n) or class I exon (n − 1) of the indicated genes. The results, calculated as the

(legend continued on next page)

(Figure 5H), demonstrating a direct role of DDX5 in miR-181b induction.

Our results revealed that DDX5 and DDX17 directly promote the expression of differentiation-specific miRNAs that in turn directly downregulate their expression. Supporting a model in which miRNA-mediated DDX5/DDX17 downregulation drives a specific splicing program, ectopic overexpression of miR-1 or miR-206 in C2C12 cells, or miR-181b in MCF10A cells induced a splicing pattern similar to that observed after cell differentiation and DDX5/DDX17 depletion (compare Figures 4G and 5I with Figures 4D and 5J).

DDX5 and DDX17 Directly Control the Transcriptional Activation of Secondary Master Transcription Factors of Cell Differentiation

Although the expression of DDX5 and DDX17 is downregulated during EMT and myogenesis, their presence is required for early steps of cell differentiation. In addition to their role in regulating the production of differentiation-specific miRNAs, we found that, in line with previous observations (Caretti et al., 2006), *Ddx5/Ddx17* knockdown in C2C12 cells also inhibited the MyoD-dependent expression of *Myog* and *Mef2c*, two master myogenic regulators (Figure 6A). This effect was most likely direct, since Ddx5 was recruited on the promoters of *Myog* and *Mef2c* genes (Figure 6A, right). As expected, Ddx5/Ddx17 depletion compromised the formation of myotubes (Figure 6B), confirming their key function in myogenesis.

Likewise, *DDX5/DDX17* knockdown prior to TGF-β treatment inhibited, at both RNA and protein levels, the TGF-β-induced and SMAD2/3-dependent expression of *SNAI1* and *SNAI2*, two master regulators of EMT (Thiery et al., 2009; Figures 6C and S6A). This effect was direct, as DDX5 was recruited on *SNAI1* and *SNAI2* promoters (Figure 6C, right), along with SMAD4 (Figure S6B). As expected, SNAIL1/2-target genes were not properly regulated by TGF-β in DDX5/DDX17-depleted cells. This included genes coding for proteins involved in epithelial cell junctions, such as Occludin and E-Cadherin (Figures S6C and S6D). As a consequence, the SNAIL-dependent loss of epithelial cell junctions, which is normally induced by TGF-β (Cano et al., 2000), and the expression of mesenchymal markers (e.g., *FAP*) were compromised in DDX5/DDX17-depleted cells (Figures 6D, S6C, and S6E). Thus, DDX5 and DDX17 serve as key transcriptional coregulators of SMADs in mediating the induction of EMT by TGF-β.

Collectively, these results support a model in which DDX5 and DDX17 cooperate with hnRNP H/F to express a specific splicing subprogram in epithelial cells and myoblasts, and are required to initiate differentiation as transcriptional coregulators of MyoD and SMAD transcription factors (Figure 7). As a consequence, they contribute to the initiation of a differentiation-specific transcription program and elicit the biogenesis of specific miRNAs, triggering a feedback control loop that contributes to the switching of splicing programs during differentiation.

DISCUSSION

Understanding alternative splicing regulation during cell differentiation is a major challenge because different cell types express different splicing isoforms that contribute to cell-specific functions (Merkin et al., 2012; Mallinjoud et al., 2014). Although the primary sequence elements of pre-mRNAs that contribute to alternative splicing are increasingly being characterized, the contribution of secondary RNA structures is far less understood (Jin et al., 2011). In this report, we propose a model in which the RNA helicase activity of DDX5 and DDX17 favors the binding of hnRNP H/F to G-tracts that can form G-quadruplex structures and assist them in their splicing-enhancer function. Supporting this model, the enhancer function of hnRNP H/F has been linked to G-runs positioned downstream of 5′ss (Wang et al., 2012b; Wang and Cambi, 2009; Xiao et al., 2009). Remarkably, if DDX5/DDX17 help the recruitment of hnRNP H/F downstream of an alternative exon defined by a weak 5′ss (class S), they enhance exon inclusion (Figure 1H) and their depletion results in exon skipping (Figures 2A–2C). However, if DDX5/DDX17 and hnRNP H/F cooperate at the level of an upstream exon (n − 1), this results in the skipping of the downstream weak exon (class I; Figure 1H). In this case, depletion of DDX5/DDX17 and/or hnRNP H/F favors the inclusion of the weak downstream exon (Figures 2D and 2E). This effect is in agreement with recent kinetic models of splicing regulation (Schor et al., 2013). Indeed, if splicing between two exons is efficient, weak internal exons are skipped and are recognized only when the splicing process is slowed down. Supporting this model, depletion of TIA1/TIAL1 splicing activators, which act downstream of weak exons (Wang et al., 2010b), inhibited the exon inclusion pattern induced by DDX5/DDX17 depletion (Figures 2F and 2G).

Our data indicate that the cooperation between DDX5/DDX17 and hnRNP H/F helps to maintain epithelial- and myoblast-specific splicing subprograms, as some of the exons that are regulated during EMT and myoblast differentiation are under the control of these factors (Figure 4). In this context, it must be underlined that exons regulated during EMT are flanked by hnRNP H/F binding motifs (Shapiro et al., 2011) and that a function of hnRNP H/F in muscle cells has previously been reported (Chen et al., 1999; Paul et al., 2011). Since DDX5 and DDX17 contribute to maintain epithelial- and myoblast-specific splicing subprograms, their downregulation during EMT and myogenesis may favor the switch toward the previously reported fibroblast- and myotube-specific splicing programs (Bland et al., 2010; Shapiro et al., 2011). Even though there is a strong overlap between DDX5/DDX17- and hnRNP H/F-regulated exons, as we observed that at least 159 of the 372 DDX5/DDX17-regulated exons in MCF7 cells are

percentage of input RNA, are represented as the mean values of at least three independent experiments ($n \geq 3$) and normalized to the control sample (IP in the presence of control siRNA), which was arbitrarily set to 1 ± SD (paired Student's t test: *$p < 0.05$).

(F) Splicing rescue experiments. Stable MCF7 cells were transfected with si*DDX5/17*-UTR and treated with doxycycline to induce the expression of wild-type DDX5 or the RNA helicase mutant DDX5-KA. One representative experiment is shown (n = 3). Quantification is shown as the fold change of psi relative to the control sample.

See also Figure S1H.

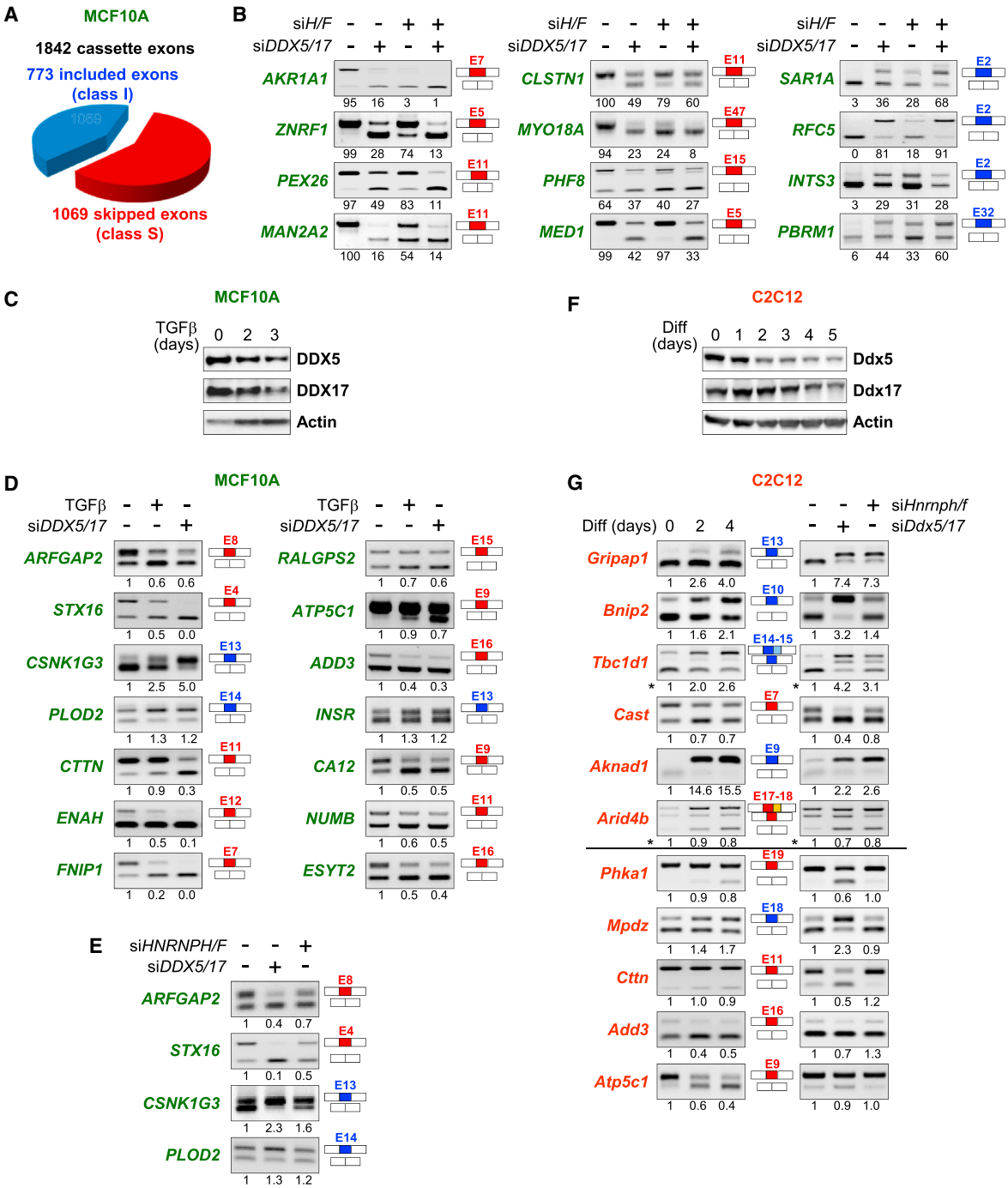

Figure 4. DDX5/DDX17 and hnRNP H/F Control the Splicing of a Subset of Exons in Epithelial Cells and Myoblasts

(A) Diagram showing the number of skipped (class S, red) and included (class I, blue) exons upon silencing of *DDX5* and *DDX17* in MCF10A cells.

(B) RT-PCR analysis of the effect of DDX5/DDX17 and hnRNP H/F on the splicing of a subset of alternative exons in MCF10A cells.

(C) Expression of DDX5 and DDX17 in TGF-β-treated MCF10A cells. Actin: loading control.

(D) Splicing of alternative exons in MCF10A cells treated with TGF-β or si*DDX5/17*. Quantification is shown as the fold change of psi relative to the control sample.

(E) Effect of hnRNP H/F on the splicing of TGF-β-induced and DDX5/DDX17-regulated exons.

(F) Expression of Ddx5 and Ddx17 during a time-course differentiation of C2C12 cells. Actin: loading control.

(G) Splicing of alternative exons in C2C12 cells induced to differentiate (left panel) or treated with si*Ddx5/17* (right panel). The black line separates exons that are coregulated or not by hnRNP H/F. Quantification as in (D). *The two upper bands were quantified together as included forms.

See also Figures S2 and S3, and Table S3.

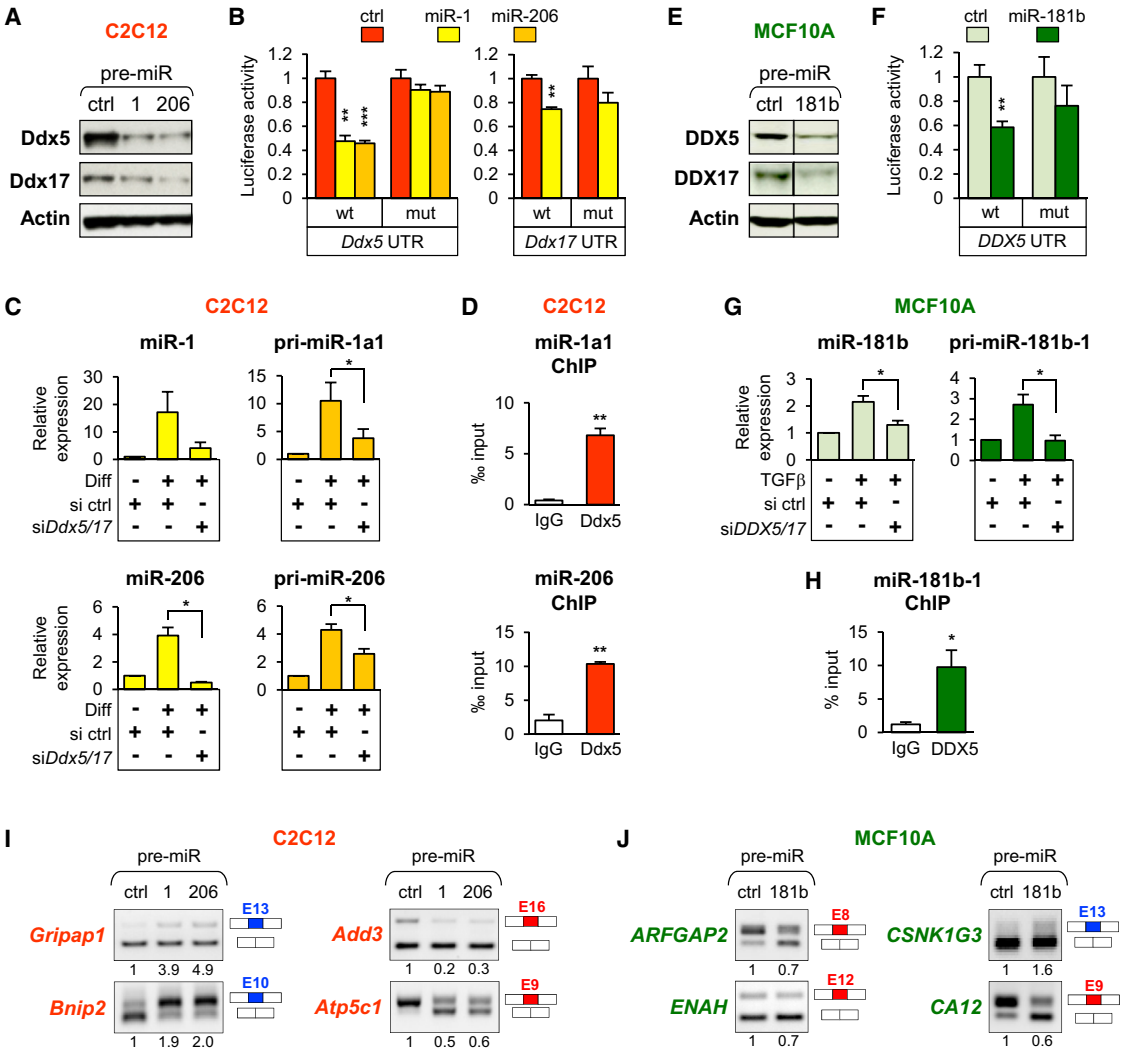

Figure 5. A Negative Feedback Loop Involving miRNAs Regulates DDX5/DDX17 Expression during Differentiation

(A) Expression of Ddx5 and Ddx17 in C2C12 cells overexpressing pre-miR-1, pre-miR-206, or a control pre-miR.

(B) Luciferase assays measuring the effect of miR-1 or miR-206 on wild-type and mutated mouse *Ddx5* and *Ddx17* 3′ UTR.

(C) Expression of miR-1 (top panel) and miR-206 (bottom panel) in C2C12 cells. Mature miRNA (yellow) or pri-miRNA (orange) were quantified 24 hr after differentiation of cells pretreated with control siRNA or si*Ddx5/17*. Values were normalized to undifferentiated cells.

(D) ChIP experiment showing Ddx5 binding to mmu-*miR-1a-1* (top) and mmu-*miR-206* (bottom) promoters.

(E) Expression of DDX5 and DDX17 in TGF-β-treated MCF10A cells overexpressing pre-miR-181b or a control pre-miRNA.

(F) Luciferase assays measuring the effect of miR-181b on wild-type and mutated human *DDX5* 3′ UTR. Details are as described in (B).

(G) Expression of mature miR-181b (light blue) and pri-miR-181b (dark blue) in MCF10A cells treated or not with TGF-β for 24 hr. Details as in (C).

(H) ChIP experiment showing DDX5 binding to the miR-181b promoter in MCF10A cells after 2 hr of TGF-β treatment.

(I) Alternative splicing in C2C12 cells ectopically expressing miR-1 or miR-206.

(J) Alternative splicing in MCF10A cells treated or not with TGF-β for 24 hr. Histograms represent a mean of at least three independent experiments ± SD (ChIP: technical qPCR replicates of one representative experiment out of three carried out independently). Student's t test: *$p < 0.05$, **$p < 0.01$, ***$p < 0.001$.

See also Figures S4 and S5.

similarly regulated by hnRNP H/F and/or contain hnRNP H/F CLIP sequences (Figures 1 and 2; Table S2), DDX5/DDX17 could have a wide impact on alternative splicing during EMT and myogenesis by modulating the activity of several other splicing factors. For example, DDX5 and DDX17 have been shown to work with RBM4 and MBNL, which are involved in the control of myogenesis (Kar et al., 2011; Laurent et al., 2012; Lin and Tarn, 2011).

Interestingly, one of the main phenotypes observed in both epithelial and myoblast cells under DDX5/DDX17 depletion was the formation of lamellipodia (Figure S7A; movies are also viewable on our website, https://fasterdb.lyon.unicancer.fr/dardenne/), which characterize motile mesenchymal cells and contribute to the alignment and fusion of myoblasts. Several genes that were spliced similarly upon DDX5/DDX17

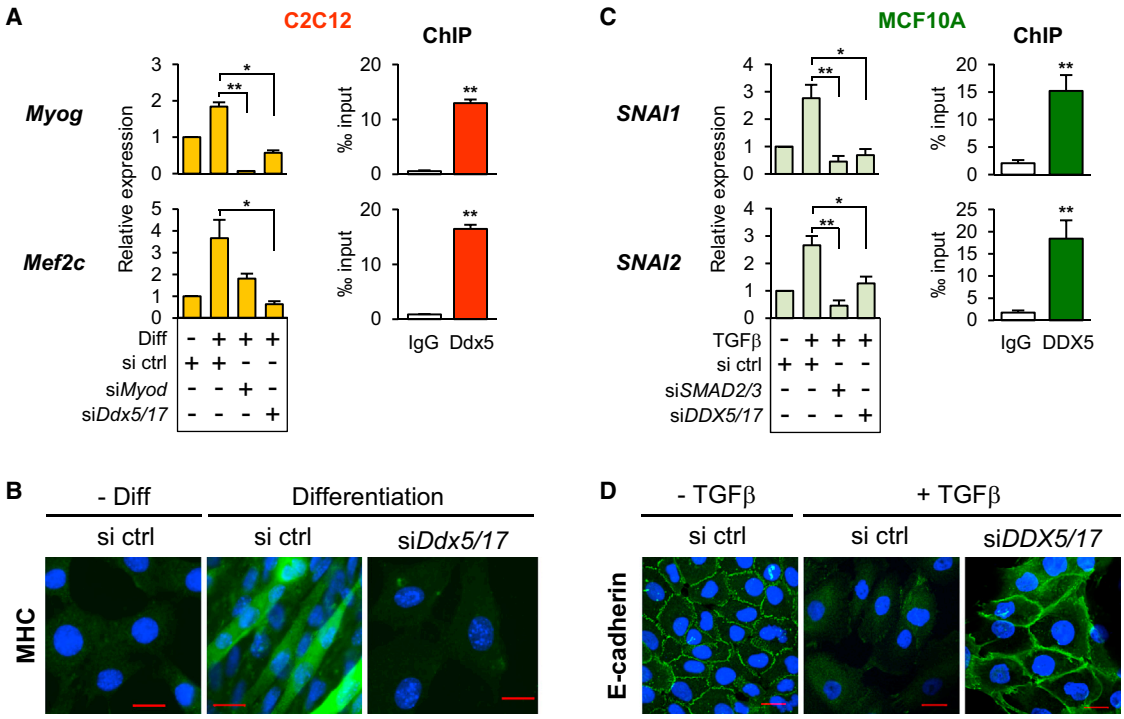

Figure 6. DDX5 and DDX17 Control the Expression of Master Transcriptional Regulators of EMT and Myogenesis

(A) qRT-PCR analysis of *Myog* and *Mef2c* in C2C12 cells after treatment with control siRNA, si*Myod*, or si*Ddx5/17*, followed by incubation in growth (− Diff) or differentiation (Diff) medium. Right panel: ChIP experiment showing Ddx5 binding to *Myog* and *Mef2c* promoters in differentiating C2C12 cells.

(B) Immunolabeling of C2C12 cells with an anti-myosin heavy chain (MHC) antibody. Scale bar, 20 μm.

(C) qRT-PCR analysis of *SNAI1* and *SNAI2* in MCF10A cells after treatment with control siRNA, si*SMAD2/3*, or si*DDX5/17*, followed or not by a 24 hr treatment with TGF-β. Right panel: ChIP experiment showing DDX5 binding to *SNAI1* and *SNAI2* promoters in MCF10A after 2 hr of TGF-β treatment. Histograms in (A) and (C) represent the mean values of at least three independent experiments normalized to the control sample ± SD (Student's t test: *$p < 0.05$, **$p < 0.01$).

(D) Immunolabeling of MCF10A cell junctions with an anti-E-cadherin antibody. Scale bar, 20 μm.

See also Figure S6.

downregulation and during EMT or myoblast differentiation are involved in actin cytoskeleton dynamics (Figure S7B), a process that is closely linked to lamellipodia formation. This suggests that splicing changes elicited by DDX5/DDX17 downregulation participate in this phenotypic change. However, other mechanisms are likely involved, as DDX5 controls, for example, the expression of miR-182, which directly affects the reorganization of the actin cytoskeleton (Wang et al., 2012a).

Finally, our data demonstrate that DDX5 and DDX17 are required not only for maintaining epithelial- and myoblast-specific splicing programs but also for initiating EMT and myogenesis owing to their role in transcription. Indeed, in agreement with previous reports (Caretti et al., 2006; Warner et al., 2004), we demonstrate that DDX5/DDX17 are transcriptional coregulators of the MyoD and SMAD transcription factors that drive transcription programs during myogenesis and TGF-β-induced EMT. One consequence of this cooperation is the production of differentiation-specific miRNAs that in turn decrease the expression of DDX5/DDX17 (Figure 5). Interestingly, our data indicate that in addition to playing a role in miRNA processing, as previously reported (Suzuki et al., 2009; Hong et al., 2013), DDX5 and DDX17 control miRNA production at the transcriptional level (Figure 5).

Altogether, our results confirmed the previously reported various regulatory functions of the RNA helicases DDX5 and DDX17 in transcription, splicing, and miRNA biogenesis (Fuller-Pace and Moore, 2011; Janknecht, 2010). However, our work unraveled a direct and dynamic orchestration of those gene-expression layers by DDX5 and DDX17 during cell differentiation. The DDX5/DDX17-dependent genetic circuitries that we characterized in two different species and biological processes are remarkably similar (Figure 7), and we propose to define such factors as master orchestrators of differentiation. It will be interesting to determine whether other DEAD box RNA helicases that are closely related to DDX5/DDX17 (such as DDX3X, DDX4/VASA, and DHX9/RHA) and also regulate different levels of gene expression in a variety of biological processes (Linder and Jankowsky, 2011) may have such a broad function in coordinating the genetic programs that unfold during biological transitions or cell differentiation processes.

EXPERIMENTAL PROCEDURES

Cell Culture, Treatment, and Transfection

Cell culture of standard and stable MCF7 cells, as well as transient transfection assays in all cell lines, was performed essentially as described previously

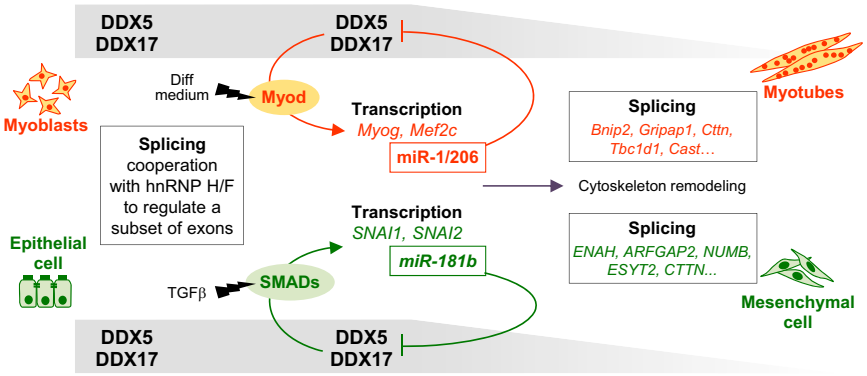

Figure 7. Orchestrated Regulation of Gene Expression by DDX5 and DDX17 during Cell Differentiation

The top (orange) and bottom (green) schemes represent the differentiation of C2C12 cells into myotubes and the TGF-β-induced EMT of MCF10A cells, respectively. In myoblasts and epithelial cells, DDX5 and DDX17 cooperate with hnRNP H/F to control the splicing of a specific subset of exons. Upon induction of differentiation, DDX5 and DDX17 coregulate MyoD- or SMAD-dependent transcriptional activity, directly controlling key effectors of differentiation, including miRNAs that in turn directly repress the expression of both helicases. DDX5 and DDX17 downregulation contributes to cell-specific variations in the alternative splicing program and to phenotypic changes that occur during differentiation, such as the formation of lamellipodia.

See also Figure S7.

(Dardenne et al., 2012; Samaan et al., 2014). Details regarding the culture of C2C12 and MCF10A cells are given in Supplemental Experimental Procedures. Sequences of the siRNAs are provided in Table S4. Pre-miRNA Precursors (Life Technologies) were used at a final concentration of 10 nM. For the analysis of the impact of potential G-quadruplexes on splicing, MCF7 cells were treated for 48 hr with 150 μM TMPyP4, a molecule that stabilizes G-quadruplexes.

Luciferase Assays

Luciferase assays using DDX5 or DDX17 reporters cloned in the psiCHEK-2 plasmid (Promega) were carried out using the Dual-Luciferase Reporter Assay System (Promega) as detailed in Supplemental Experimental Procedures.

RNA Analysis

RNA extraction, RT-PCR, and quantitative RT-PCR (qRT-PCR) were performed as described previously (Dardenne et al., 2012; Samaan et al., 2014). The primer sequences for PCR and qPCR are provided in Table S4. Quantification of mature miRNAs was carried out using the miRCURY LNA Universal cDNA synthesis and SYBR Green PCR kit (Exiqon), with specific LNA primer sets, according to the manufacturer's instructions. qRT-PCR values were normalized relative to U6 snRNA.

Chromatin and RNA Immunoprecipitation

Chromatin immunoprecipitations (ChIPs) were performed as previously described (Fattet et al., 2013; Zonta et al., 2013) using antibodies against DDX5 (4 μg, A300-523A; Bethyl), SMAD4 (sc-7154; Santa Cruz), or control immunoglobulin G (IgG, sc-2027; Santa Cruz). RNA-IP was performed as previously described (Bittencourt et al., 2008) using hnRNP H1 antibodies (A300-511A; Bethyl) or rabbit IgG (sc-2027; Santa Cruz).

Microscopy

Details regarding the protocols used for immunofluorescence, in situ PLAs, and time-lapse videomicroscopy are given in Supplemental Experimental Procedures.

Bioinformatics

Microarray analyses were performed as described previously (Mallinjoud et al., 2014). Exon numbering of mouse and human genes was based on the FasterDB annotation (https://fasterdb.lyon.unicancer.fr/index.php).

MaxEntScan was used to measure the scores of the 5′ss and 3′ss. SFmap web server (http://sfmap.technion.ac.il/) (Paz et al., 2010) was used to predict and map known splicing-factor binding sites. The UCSC LiftOver tool (http://genome.ucsc.edu/cgi-bin/hgLiftOver) was used to look at conservation between human and mouse exons.

Publicly available CLIP-seq data sets were retrieved from the NCBI Gene Expression Omnibus for hnRNPH1 and hnRNPF (GSE23694 and GSE34993), and from ArrayExpress for TIA and TIAL1 (E-MTAB-432). The number of reads that overlapped the regions of interest was computed using coverageBed (Bedtools).

For the prediction of G-quadruplex structures, the first 50 or 60 intronic nucleotides downstream of the exons of interest were searched for the previously described alternative G-quadruplex motif $G_{n>2}$-$(N_{1-7}$-$G_{n>2})_3$ (Xiao et al., 2013). Each sequence position was associated to the number of G-quadruplexes that overlap this nucleotide. The data points were then binned to smooth the curve (bin size set to 5).

ACCESSION NUMBERS

The raw microarray data for the *DDX5*/*DDX17* silencing experiments performed in MCF7 and MCF10A cells have been deposited in the NCBI Gene Expression Omnibus under accession number GSE57281.

SUPPLEMENTAL INFORMATION

Supplemental Information includes Supplemental Experimental Procedures, seven figures, and four tables and can be found with this article online at http://dx.doi.org/10.1016/j.celrep.2014.05.010.

AUTHOR CONTRIBUTIONS

E.D. performed experiments and analyzed data. M.P.E. performed experiments and bioinformatic analyses, and analyzed data. L.F., S.G., M.-P.L., H.N., E.Z., L.G., M. Deygas, F.Z.C., and S.S. performed experiments and analyzed data. H.M., F.-O.D., and L.-C.T. performed bioinformatic analyses. R.R. designed experiments and analyzed data. M. Dutertre analyzed data and edited the paper. C.F.B. designed and performed experiments, analyzed data, and co-wrote the paper. D.A. designed experiments, analyzed data, and co-wrote the paper. All authors gave input on the paper.

ACKNOWLEDGMENTS

We are grateful to D. Furling and J. Marie for their comments on the manuscript. We thank C. Vanbelle and C. Bouchardon (CIQLE-SFR Santé Lyon-Est) and Dr. Joël Lachuer (ProfileXpert-LCMT Facility, Lyon, France) for their assistance with imaging and microarray analyses, respectively. This work was supported by grants from INSERM "Plan Cancer 2009-2013," INCa, the Fondation pour la Recherche Médicale (FRM) and LNCC, and AFM-Téléthon. It was also supported by doctoral fellowships from the LNCC (E.D.), AFM (M.P.E.), French Ministère de l'Enseignement Supérieur et de la Recherche (L.F. and M.D.), and FRM (E.Z.), and postdoctoral fellowships from the Centre Léon Bérard (H.N.), FRM (H.M.), and Fondation ARC (S.G., M.P.L., F.Z.C., F.-O.D., and L.-C.T.).

Received: October 25, 2013
Revised: April 8, 2014
Accepted: May 5, 2014
Published: June 5, 2014

REFERENCES

Bittencourt, D., Dutertre, M., Sanchez, G., Barbier, J., Gratadou, L., and Auboeuf, D. (2008). Cotranscriptional splicing potentiates the mRNA production from a subset of estradiol-stimulated genes. Mol. Cell. Biol. *28*, 5811–5824.

Bland, C.S., Wang, E.T., Vu, A., David, M.P., Castle, J.C., Johnson, J.M., Burge, C.B., and Cooper, T.A. (2010). Global regulation of alternative splicing during myogenic differentiation. Nucleic Acids Res. *38*, 7651–7664.

Camats, M., Guil, S., Kokolo, M., and Bach-Elias, M. (2008). P68 RNA helicase (DDX5) alters activity of cis- and trans-acting factors of the alternative splicing of H-Ras. PLoS ONE *3*, e2926.

Cano, A., Pérez-Moreno, M.A., Rodrigo, I., Locascio, A., Blanco, M.J., del Barrio, M.G., Portillo, F., and Nieto, M.A. (2000). The transcription factor snail controls epithelial-mesenchymal transitions by repressing E-cadherin expression. Nat. Cell Biol. *2*, 76–83.

Caretti, G., Schiltz, R.L., Dilworth, F.J., Di Padova, M., Zhao, P., Ogryzko, V., Fuller-Pace, F.V., Hoffman, E.P., Tapscott, S.J., and Sartorelli, V. (2006). The RNA helicases p68/p72 and the noncoding RNA SRA are coregulators of MyoD and skeletal muscle differentiation. Dev. Cell *11*, 547–560.

Chen, C.D., Kobayashi, R., and Helfman, D.M. (1999). Binding of hnRNP H to an exonic splicing silencer is involved in the regulation of alternative splicing of the rat beta-tropomyosin gene. Genes Dev. *13*, 593–606.

Dardenne, E., Pierredon, S., Driouch, K., Gratadou, L., Lacroix-Triki, M., Espinoza, M.P., Zonta, E., Germann, S., Mortada, H., Villemin, J.P., et al. (2012). Splicing switch of an epigenetic regulator by RNA helicases promotes tumor-cell invasiveness. Nat. Struct. Mol. Biol. *19*, 1139–1146.

Davis, B.N., Hilyard, A.C., Lagna, G., and Hata, A. (2008). SMAD proteins control DROSHA-mediated microRNA maturation. Nature *454*, 56–61.

Decorsière, A., Cayrel, A., Vagner, S., and Millevoi, S. (2011). Essential role for the interaction between hnRNP H/F and a G quadruplex in maintaining p53 pre-mRNA 3′-end processing and function during DNA damage. Genes Dev. *25*, 220–225.

Ebert, M.S., and Sharp, P.A. (2012). Roles for microRNAs in conferring robustness to biological processes. Cell *149*, 515–524.

Fattet, L., Ay, A.S., Bonneau, B., Jallades, L., Mikaelian, I., Treilleux, I., Gillet, G., Hesling, C., and Rimokh, R. (2013). TIF1γ requires sumoylation to exert its repressive activity on TGFβ signaling. J. Cell Sci. *126*, 3713–3723.

Fukuda, T., Yamagata, K., Fujiyama, S., Matsumoto, T., Koshida, I., Yoshimura, K., Mihara, M., Naitou, M., Endoh, H., Nakamura, T., et al. (2007). DEAD-box RNA helicase subunits of the Drosha complex are required for processing of rRNA and a subset of microRNAs. Nat. Cell Biol. *9*, 604–611.

Fuller-Pace, F.V., and Moore, H.C. (2011). RNA helicases p68 and p72: multifunctional proteins with important implications for cancer development. Future Oncol. *7*, 239–251.

Germann, S., Gratadou, L., Zonta, E., Dardenne, E., Gaudineau, B., Fougère, M., Samaan, S., Dutertre, M., Jauliac, S., and Auboeuf, D. (2012). Dual role of the ddx5/ddx17 RNA helicases in the control of the pro-migratory NFAT5 transcription factor. Oncogene *31*, 4536–4549.

Hong, S., Noh, H., Chen, H., Padia, R., Pan, Z.K., Su, S.B., Jing, Q., Ding, H.F., and Huang, S. (2013). Signaling by p38 MAPK stimulates nuclear localization of the microprocessor component p68 for processing of selected primary microRNAs. Sci. Signal. *6*, ra16.

Huelga, S.C., Vu, A.Q., Arnold, J.D., Liang, T.Y., Liu, P.P., Yan, B.Y., Donohue, J.P., Shiue, L., Hoon, S., Brenner, S., et al. (2012). Integrative genome-wide analysis reveals cooperative regulation of alternative splicing by hnRNP proteins. Cell Reports *1*, 167–178.

Janknecht, R. (2010). Multi-talented DEAD-box proteins and potential tumor promoters: p68 RNA helicase (DDX5) and its paralog, p72 RNA helicase (DDX17). Am. J. Transl. Res. *2*, 223–234.

Jin, Y., Yang, Y., and Zhang, P. (2011). New insights into RNA secondary structure in the alternative splicing of pre-mRNAs. RNA Biol. *8*, 450–457.

Kalsotra, A., and Cooper, T.A. (2011). Functional consequences of developmentally regulated alternative splicing. Nat. Rev. Genet. *12*, 715–729.

Kar, A., Fushimi, K., Zhou, X., Ray, P., Shi, C., Chen, X., Liu, Z., Chen, S., and Wu, J.Y. (2011). RNA helicase p68 (DDX5) regulates tau exon 10 splicing by modulating a stem-loop structure at the 5′ splice site. Mol. Cell. Biol. *31*, 1812–1821.

Katz, Y., Wang, E.T., Airoldi, E.M., and Burge, C.B. (2010). Analysis and design of RNA sequencing experiments for identifying isoform regulation. Nat. Methods *7*, 1009–1015.

Laurent, F.X., Sureau, A., Klein, A.F., Trouslard, F., Gasnier, E., Furling, D., and Marie, J. (2012). New function for the RNA helicase p68/DDX5 as a modifier of MBNL1 activity on expanded CUG repeats. Nucleic Acids Res. *40*, 3159–3171.

Lim, L.P., and Burge, C.B. (2001). A computational analysis of sequence features involved in recognition of short introns. Proc. Natl. Acad. Sci. USA *98*, 11193–11198.

Lin, J.C., and Tarn, W.Y. (2011). RBM4 down-regulates PTB and antagonizes its activity in muscle cell-specific alternative splicing. J. Cell Biol. *193*, 509–520.

Lin, C., Yang, L., Yang, J.J., Huang, Y., and Liu, Z.R. (2005). ATPase/helicase activities of p68 RNA helicase are required for pre-mRNA splicing but not for assembly of the spliceosome. Mol. Cell. Biol. *25*, 7484–7493.

Linder, P., and Jankowsky, E. (2011). From unwinding to clamping—the DEAD box RNA helicase family. Nat. Rev. Mol. Cell Biol. *12*, 505–516.

Mallinjoud, P., Villemin, J.P., Mortada, H., Polay Espinoza, M., Desmet, F.O., Samaan, S., Chautard, E., Tranchevent, L.C., and Auboeuf, D. (2014). Endothelial, epithelial, and fibroblast cells exhibit specific splicing programs independently of their tissue of origin. Genome Res. *24*, 511–521.

Merkin, J., Russell, C., Chen, P., and Burge, C.B. (2012). Evolutionary dynamics of gene and isoform regulation in mammalian tissues. Science *338*, 1593–1599.

Paul, S., Dansithong, W., Jog, S.P., Holt, I., Mittal, S., Brook, J.D., Morris, G.E., Comai, L., and Reddy, S. (2011). Expanded CUG repeats dysregulate RNA splicing by altering the stoichiometry of the muscleblind 1 complex. J. Biol. Chem. *286*, 38427–38438.

Paz, I., Akerman, M., Dror, I., Kosti, I., and Mandel-Gutfreund, Y. (2010). SFmap: a web server for motif analysis and prediction of splicing factor binding sites. Nucleic Acids Res. *38*, W281–W285.

Rao, P.K., Kumar, R.M., Farkhondeh, M., Baskerville, S., and Lodish, H.F. (2006). Myogenic factors that regulate expression of muscle-specific microRNAs. Proc. Natl. Acad. Sci. USA *103*, 8721–8726.

Samaan, S., Tranchevent, L.C., Dardenne, E., Polay Espinoza, M., Zonta, E., Germann, S., Gratadou, L., Dutertre, M., and Auboeuf, D. (2014). The Ddx5 and Ddx17 RNA helicases are cornerstones in the complex regulatory array of steroid hormone-signaling pathways. Nucleic Acids Res. *42*, 2197–2207.

Samatanga, B., Dominguez, C., Jelesarov, I., and Allain, F.H. (2013). The high kinetic stability of a G-quadruplex limits hnRNP F qRRM3 binding to G-tract RNA. Nucleic Acids Res. *41*, 2505–2516.

Schor, I.E., Gómez Acuña, L.I., and Kornblihtt, A.R. (2013). Coupling between transcription and alternative splicing. Cancer Treat. Res. *158*, 1–24.

Shapiro, I.M., Cheng, A.W., Flytzanis, N.C., Balsamo, M., Condeelis, J.S., Oktay, M.H., Burge, C.B., and Gertler, F.B. (2011). An EMT-driven alternative splicing program occurs in human breast cancer and modulates cellular phenotype. PLoS Genet. *7*, e1002218.

Suzuki, H.I., Yamagata, K., Sugimoto, K., Iwamoto, T., Kato, S., and Miyazono, K. (2009). Modulation of microRNA processing by p53. Nature *460*, 529–533.

Thiery, J.P., Acloque, H., Huang, R.Y., and Nieto, M.A. (2009). Epithelial-mesenchymal transitions in development and disease. Cell *139*, 871–890.

Wang, E., and Cambi, F. (2009). Heterogeneous nuclear ribonucleoproteins H and F regulate the proteolipid protein/DM20 ratio by recruiting U1 small nuclear ribonucleoprotein through a complex array of G runs. J. Biol. Chem. *284*, 11194–11204.

Wang, B., Hsu, S.H., Majumder, S., Kutay, H., Huang, W., Jacob, S.T., and Ghoshal, K. (2010a). TGFbeta-mediated upregulation of hepatic miR-181b promotes hepatocarcinogenesis by targeting TIMP3. Oncogene *29*, 1787–1797.

Wang, Z., Kayikci, M., Briese, M., Zarnack, K., Luscombe, N.M., Rot, G., Zupan, B., Curk, T., and Ule, J. (2010b). iCLIP predicts the dual splicing effects of TIA-RNA interactions. PLoS Biol. *8*, e1000530.

Wang, D., Huang, J., and Hu, Z. (2012a). RNA helicase DDX5 regulates microRNA expression and contributes to cytoskeletal reorganization in basal breast cancer cells. Mol. Cell. Proteomics *11*, M111.011932.

Wang, E., Aslanzadeh, V., Papa, F., Zhu, H., de la Grange, P., and Cambi, F. (2012b). Global profiling of alternative splicing events and gene expression regulated by hnRNPH/F. PLoS ONE *7*, e51266.

Warner, D.R., Bhattacherjee, V., Yin, X., Singh, S., Mukhopadhyay, P., Pisano, M.M., and Greene, R.M. (2004). Functional interaction between Smad, CREB binding protein, and p68 RNA helicase. Biochem. Biophys. Res. Commun. *324*, 70–76.

Warzecha, C.C., Jiang, P., Amirikian, K., Dittmar, K.A., Lu, H., Shen, S., Guo, W., Xing, Y., and Carstens, R.P. (2010). An ESRP-regulated splicing programme is abrogated during the epithelial-mesenchymal transition. EMBO J. *29*, 3286–3300.

Xiao, X., Wang, Z., Jang, M., Nutiu, R., Wang, E.T., and Burge, C.B. (2009). Splice site strength-dependent activity and genetic buffering by poly-G runs. Nat. Struct. Mol. Biol. *16*, 1094–1100.

Xiao, S., Zhang, J.Y., Zheng, K.W., Hao, Y.H., and Tan, Z. (2013). Bioinformatic analysis reveals an evolutional selection for DNA:RNA hybrid G-quadruplex structures as putative transcription regulatory elements in warm-blooded animals. Nucleic Acids Res. *41*, 10379–10390.

Yang, L., Lin, C., and Liu, Z.R. (2006). P68 RNA helicase mediates PDGF-induced epithelial mesenchymal transition by displacing Axin from beta-catenin. Cell *127*, 139–155.

Zhang, X.H., Leslie, C.S., and Chasin, L.A. (2005). Dichotomous splicing signals in exon flanks. Genome Res. *15*, 768–779.

Zonta, E., Bittencourt, D., Samaan, S., Germann, S., Dutertre, M., and Auboeuf, D. (2013). The RNA helicase DDX5/p68 is a key factor promoting c-fos expression at different levels from transcription to mRNA export. Nucleic Acids Res. *41*, 554–564.